Development and *In Vivo* Performance Evaluation of 10–60-MHz Band Impulse-Radio-Based Transceiver for Deep Implantation Having 10 Mb/s

Jianqing Wang, *Member, IEEE*, Kohei Nomura, Hiroki Narita, Fuminori Ito, Daisuke Anzai, *Member, IEEE*, Jacob Bergsland, and Ilangko Balasingham, *Senior Member, IEEE*

***Abstract*— In view of the requirements for high-speed highly reliable wireless implant communication, we have developed an implant transceiver working at a 10–60-MHz band. The developed transceiver is based on an impulse radio technology with multipulse position modulation to increase the communication speed and reliability, and utilizes the automatic equalization technique to suppress waveform distortion and intersymbol interference due to frequency-dependent tissue properties. The transmit antenna has a dimension of 2.6 cm × 1.6 cm × 1.6 cm and a relative bandwidth of 16% by forming the radiation elements on a flexible magnetic sheet for miniaturization. Through an *in vivo* experiment on a living swine, we have shown the feasibility of implant communication in a depth up to 26 cm with a minimum data rate of 10 Mb/s. These results demonstrate the superiority of this new technology over all others reported so far in the literature.**

***Index Terms*— Automatic equalization, implant antenna, implant transceiver, impulse radio (IR), *in vivo* experiment, wireless implant communication.**

I. Introduction

THE aging population is becoming a global social challenge. There is a strong desire to find technological solutions to provide cost-benefit, cost-effective health care services. To this end, information and communication technology can play a pivotal role in developing novel applications. For example, various types of *in vivo* biological sensors and *in vivo* medical robots can be used not only to detect biological information and images but also for long-term function in the abdominal cavity or embedded in organs for continuous diagnosis and treatment. Microrobots can eventually be expected to move freely within the human body to offer remote treatment or drug injection. To improve biosensing and actuator-driven techniques, it is essential to establish high-speed and highly reliable wireless implant communication between inside and outside of the human body [1]–[3]. Yuce and Dissanayake [4] summarized the status of implant communications. Current implant communications mainly employ the 400-MHz band. Due to the limitation of frequency regulation in this band, a narrowband modulation scheme must be adopted, which limits the available data rates to several hundred kilobits per second. Since implant communication may be used for *in vivo* image transmission, data rates as high as several megabits per second are usually required. To increase the data rate, the authors previously attempted to employ ultra-wideband (UWB) technology at its low band (3.4–4.8 GHz). However, the transmission experiment in a living swine only demonstrated a possibility to secure a bit error rate (BER) of 10^{-2} at 1 Mb/s at a depth of 5 cm [5], which is insufficient for implant applications. Although it was attempted to combine transmit diversity and receive diversity to achieve higher data rate [6], no significant improvement on the communication distance was achieved in the body.

The human body is a lossy dielectric medium. The wavelength inside it is shortened due to its frequency-dependent dielectric properties. The dielectric properties are usually expressed using the complex permittivity, which is a summation of terms corresponding to various dispersion mechanisms. Four Debye-type dispersion expressions provide good modeling for most human tissues. The corresponding expression of the complex permittivity as a function of angle frequency ω is given as [7]

$$\dot{\varepsilon_r}(\omega) = \varepsilon_\infty + \sum_{n=1}^{4} \frac{\Delta\varepsilon_n}{1 + (j\omega\tau_n)^{1-\alpha_n}} + \frac{\sigma_0}{j\omega\varepsilon_0} \tag{1}$$

where each term is described in terms of a modified Debye expression. In each dispersion region, $\Delta\epsilon_n$ is the magnitude of

Manuscript received February 25, 2018; revised June 8, 2018; accepted June 20, 2018. Date of publication July 23, 2018; date of current version September 4, 2018. This work was supported in part by MIC/SCOPE Japan under Grant 185006005 and in part by the Research Council of Norway through the project Wireless In-body Sensors and Actuator Networks (WINNOW) under Grant 270957/O70. *(Corresponding author: Jianqing Wang.)*

J. Wang and D. Anzai are with the Graduate School of Engineering, Nagoya Institute of Technology, Nagoya 466-8555, Japan (e-mail: wang@nitech.ac.jp).

K. Nomura was with the Graduate School of Engineering, Nagoya Institute of Technology, Nagoya 466-8555, Japan. He is now with the Mitsubishi Electric Corporation, Kobe 652-8555, Japan.

H. Narita was with the Graduate School of Engineering, Nagoya Institute of Technology, Nagoya 466-8555, Japan. He is now with Aisin Seiki Co., Ltd., Aichi 448-8650, Japan.

F. Ito was with the Graduate School of Engineering, Nagoya Institute of Technology, Nagoya 466-8555, Japan. He is now with the DENSO TECHNO Co., Ltd., Aichi 474-0025, Japan.

J. Bergsland is with the Intervention Center, Oslo University Hospital, NO-0027 Oslo, Norway.

I. Balasingham is with the Intervention Center, Oslo University Hospital, NO-0027 Oslo, Norway, and also with the Department of Electronic Systems, Norwegian University of Science and Technology, NO-7491 Trondheim, Norway.

Color versions of one or more of the figures in this paper are available online at http://ieeexplore.ieee.org.

Digital Object Identifier 10.1109/TMTT.2018.2854165

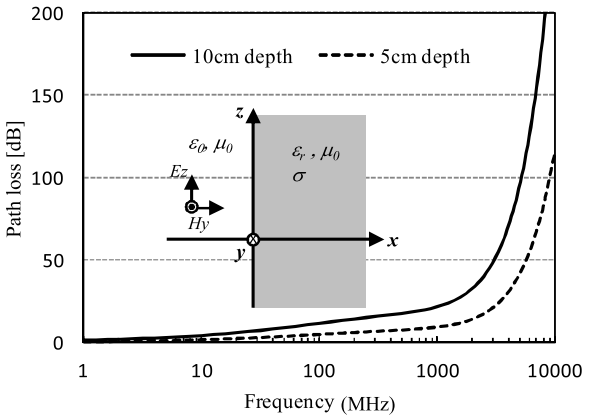

Fig. 1. Frequency dependence of path loss for muscle tissue at depths of 10 and 5 cm, respectively, for a 1-D model.

dispersion, τ_n is the relaxation time constant, α_n is the deviation from Debye behavior. ϵ_0 is the free-space permittivity, ϵ_∞ is the permittivity when the frequency approaches infinity, and σ_0 is the ionic conductivity. The determined parameters for each tissue are shown in [8]. The frequency-dependent dielectric properties result in severe signal attenuation and waveform distortion when a signal passes through the human body.

Fig. 1 shows a semi-infinite large plane medium of homogeneous human muscle tissue with a normal plane wave incidence to it. The corresponding path loss was calculated theoretically at two typical depth of 5 and 10 cm. Compared to the 400-MHz band and UWB band, the path loss at the 10–60-MHz band is much smaller, which can thus provide a significant improvement on the communication distance in the human body. This result suggests that the implant communication is more appropriate at lower frequencies from the point of view of path loss. In addition, the 10–60-MHz band falls in the extremely weak radio band in Japan. According to a Japanese radio law, as long as the radiated electric field intensity is lower than 500 μV/m at a distance of 3 m, it is legally available for use [9]. This requirement is actually easy to satisfy because of the implant transceiver's small size, low transmit power, and usage in lossy media. However, there are two problems that need to be resolved in employing the 10–60-MHz band for implant communication. The first is how to raise the data rate up to 10 Mb/s or higher, and the other is how to design a wideband implantable antenna with a dimension of 2–3 cm.

In this paper, we aim to develop the 10–60-MHz band implant transceiver to achieve a data rate of up to 10 Mb/s at a deep communication distance. To this end, we employ a wideband impulse radio-multipulse position modulation (IR-MPPM) scheme, together with an automatic equalizer to suppress the waveform distortion and resultant intersymbol interference. To realize a small size wideband antenna in this frequency band, we make the transmit signal that has a frequency spectrum shape favorable for antenna design, and form the antenna on a material with high magnetic permeability based on the wavelength shortening effect.

This paper is organized as follows. Section II describes the basic implant transmitter structure, signal waveforms, and frequency spectra. Section III describes the implant antenna

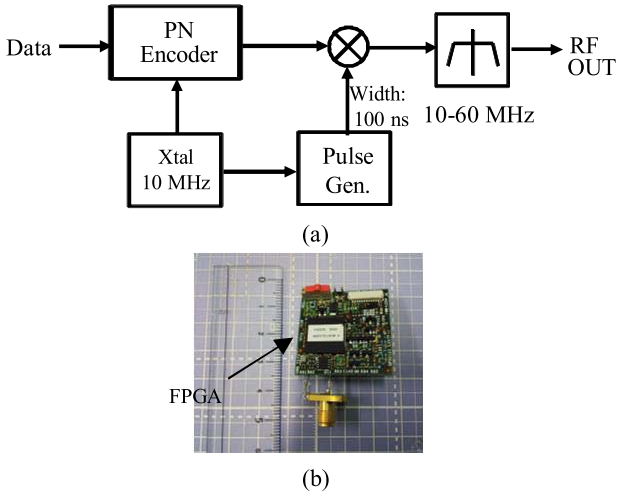

Fig. 2. (a) Structure of the IR-MPPM transmitter. (b) Hardware implementation with FPGA board. The total size is 3 cm × 3 cm.

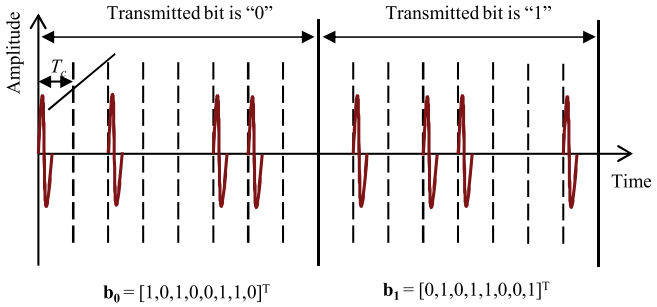

Fig. 3. Concept of the IR-MPPM with $M = 8$.

design and their performance evaluation. Section IV describes the receiver structure with automatic equalization, and Section V gives the *in vivo* communication performance evaluation results in a living swine. Section VI concludes this paper.

II. Transmitter Structure and Performance

IR technique has a potential for wideband and high-speed communication because it transmits short pulses directly based on digital bits. The feature without carrier signal also contributes to the miniaturization of the implant transmitter. Fig. 2(a) and (b) shows the structure of the implant transmitter and its hardware implementation, respectively. The digitized information bit is first encoded with a pseudonoise (pn) code, which is driven by a clock generator at 10 MHz. The pn code may consist of one chip, two chips, four chips, or eight chips, determined by the required data rate, and the chip rate is the clock frequency of 10 MHz. If one bit is encoded on one chip, the corresponding data rate is 10 Mb/s, while if one bit is encoded on eight chips, the corresponding data rate is 1.25 Mb/s. The pulse generator produces the pulse to be transmitted with a width of nearly 100 ns. When the chip is "1," the pulse is sent to the bandpass filter (BPF), while when the chip is "0," nothing is sent. This looks like an ON–OFF keying (OOK) scheme. However, since multiple chips are used to represent one information bit, for example, as shown in Fig. 3, "10100110" is used to represent information bit "0" and "01011001" is used to represent information "1," the combination of a pn encoder and OOK modulation can be considered as an MPPM scheme with $M = 8$. By adjusting

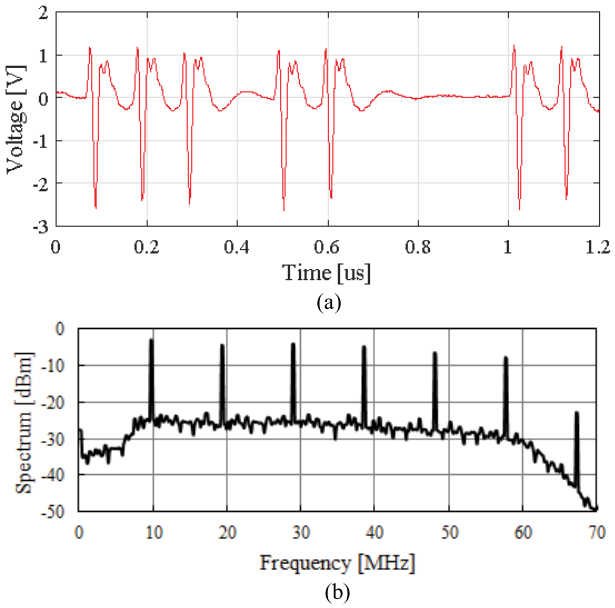

Fig. 4. Example of the transmitted signal. (a) Time waveform. (b) Frequency spectrum.

the chip number within one-bit period, the data rate can change from 1.25 ($M = 8$) to 10 Mb/s ($M = 1$). The pulse sequences modulated in such a form are then spectrum formed between 10 and 60 MHz by the BPF at the transmitter output. The transmitter was packaged on a 3 cm × 3 cm printed circuit board. Except for the crystal oscillator and the BPF, all the other parts such as the pn encoder, pulse generator, and multiplier were implemented in a commercially available field-programmable gate array (FPGA) (Xilinx, Spartan-6). With the current integrated circuit technology, it is not difficult to integrate all the parts in one chip with a smaller size for actual implant applications.

Fig. 4 shows the time waveform and signal spectrum at the transmitter output measured by a digital oscilloscope (sampling frequency: 8 GHz; bandwidth: 1.5 GHz) and a spectrum analyzer, respectively. As can be seen, the pulses have a width of nearly 100 ns, and they are sent out directly according to the pn encoder and OOK modulator. It should be emphasized that, as can be seen from the frequency spectrum, instead of making the signal components cover the entire 10–60-MHz band, we employed a pulse where the signal components were concentrated at six specific frequencies of 10, 20, 29, 39, 48, and 58 MHz. This spectrum shape was based on the consideration that it is difficult to design an antenna with a bandwidth as wide as 50 MHz with respect to the central frequency of 35 MHz (relative bandwidth of 1.4). By concentrating the signal components at the six specific frequencies, the implant antenna needs not cover the entire 10–60-MHz band. It can be designed to have a narrow bandwidth focusing on these specific frequencies. This greatly eases the difficulty in designing a wideband antenna at this frequency band.

III. Antenna Structure and Performance

The transmit antenna needs to be of small size (2–3 cm) for implant application. However, the wavelength λ_0 at the

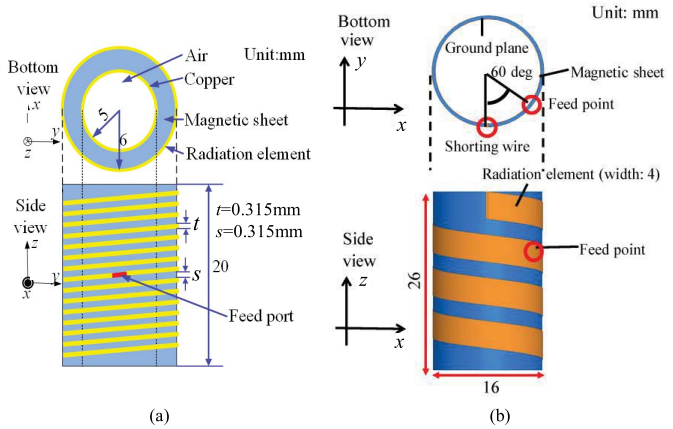

Fig. 5. Designed implant antenna structure. (a) Helical dipole structure. (b) Helical invert-F dipole structure.

10–60-MHz band is around 10 m in free space. It is essential to shorten the equivalent wavelength for antenna miniaturization. We thus utilized the wavelength shortening effect of the material's permeability and permittivity. A magnetic material may have both a high relative permeability μ_r and a high relative permittivity ε_r. Since the equivalent wavelength $\lambda \cong \lambda_0/(\varepsilon_r \mu_r)^{1/2}$, we can expect a double shortening effect by fabricating the antenna radiation element on a magnetic sheet. The flexibility of the magnetic sheet is also beneficial to form a cylindrical shape into which the transmitter circuit can be placed.

Fig. 5 shows two structures of the implant antenna design based on the above-mentioned consideration by using an electromagnetic field simulation tool of finite-element method (Ansys, HFSS). The antenna in Fig. 5(a) is a helical dipole structure with a reflection plane [10]. It has a hollow cylindrical shape and consists of three layers. In the first layer, a copper foil with a thickness of 0.1 mm forms the hollow cylinder with a radius of 5 mm, and this acts as the reflection plane of the antenna radiating elements. The second layer is a flexible magnetic sheet with a thickness of 1 mm. The flexible magnetic sheet is a commercially available one with $\mu_r = 20.7$, $\tan\delta_\mu = 0.12$, $\varepsilon_r = 13.0$, and $\tan\delta_\varepsilon = 0.17$, where $\tan\delta_\mu$ is the magnetic loss tangent and $\tan\delta_\epsilon$ is the dielectric loss tangent. The third layer consists of the two dipole elements: two copper wires with a thickness of 0.315 mm. At the two sides of the feeding point, the two wires are wrapped seven turns, respectively, with a spacing of 0.315 mm.

On the other hand, the antenna in Fig. 5(b) is a helical invert-F dipole structure. It also has a hollow cylindrical shape and consists of three layers. In the first layer, a copper foil with a thickness of 0.1 mm forms the hollow cylinder with a radius of 7.3 mm, and this plays the role of antenna ground. The second layer is the flexible magnetic sheet with a thickness of 0.5 mm, and the third layer is the radiating element formed of a copper foil with a thickness of 0.1 mm and a width of 4 mm. In order to adjust the antenna input impedance, the inverted-F antenna structure is used so that the feeding source between the radiating element and the ground is set at the upside of the cylinder and a short pin between the radiating element and the ground is set at the top of the cylinder.

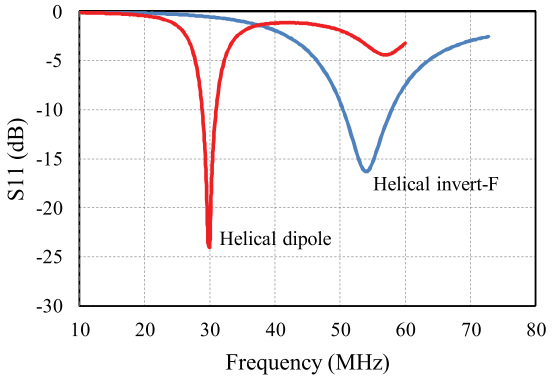

Fig. 6. Measured S_{11} characteristics versus frequency for the two antennas.

The two antennas were inserted, respectively, into a biological-equivalent liquid phantom with a dimension of 28 cm × 16 cm × 28 cm for S_{11} measurement with a network analyzer. The liquid phantom was made of deionized water, sugar, sodium chloride, and so on, and its dielectric properties were adjusted to be $\epsilon_r = 56.05$ and conductivity $\sigma = 0.52$ S/m at 30 MHz, nearly 2/3 times the muscle's values. The antennas were wrapped in vinyl for insulation from the liquid phantom. Fig. 6 shows the measured S_{11} characteristics versus frequency for the two antennas. As can be seen, the helical dipole antenna showed an absolute −10-dB bandwidth of about 2.2 MHz around 30 MHz (relative bandwidth of 7.3%), which can only effectively transmit the signal components around 29 MHz for the spectrum shape in Fig. 4(b). However, the helical invert-F dipole antenna showed an absolute −10-dB bandwidth of about 8.4 MHz (relative bandwidth of 16%). As a result, the signal components at both 48 and 58 MHz can be effectively transmitted. This suggests that the helical invert-F dipole antenna with a dimension of 2.6 cm × 1.6 cm × 1.6 cm may provide a better communication performance than the helical dipole antenna.

IV. Receiver Structure and Performance

The received signal is filtered and amplified and then adjusted to an adequate level by a gain controller. Since the signal is in a wideband, the waveform is distorted when passing through the human body due to its frequency-dependent dielectric properties. The band-limited implant antenna is also one of the reasons of waveform distortion. Therefore, an intersymbol interference is inevitable in the implant communication. In order to suppress the waveform distortion and intersymbol interference, implementation of an automatic waveform equalizer to the receiver is desired. Fig. 7(a) and (b) shows the receiver structure and its hardware implementation, respectively. The automatic equalizer, IR-MPPM demodulator, and data storage are implemented in an FPGA (Xilinx, Virtex-6) board with a total size of 26 cm × 10 cm. The analog signal is first analog–digital converted, and is then input to an automatic equalizer. As a usual equalization method, there are a minimum mean square error (mmse) method and a zero forcing (ZF) method. The mmse method minimizes the mse between the transmitted signal and the received signal. Since the amount of calculation is large, it consumes more power

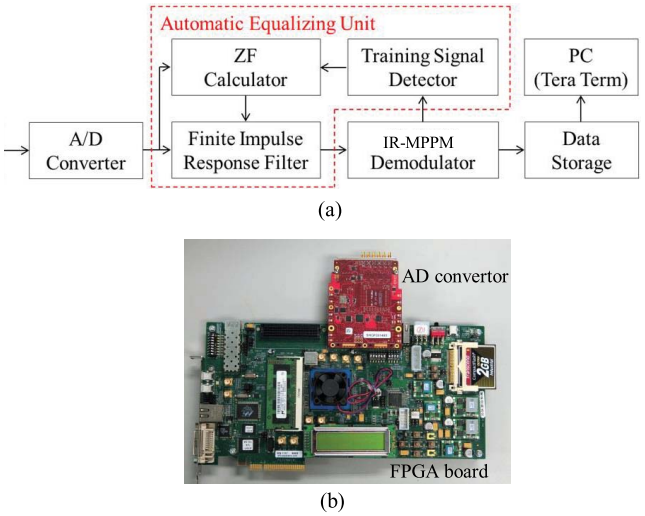

Fig. 7. (a) Structure of the receiver with automatic equalizer. (b) Hardware implementation. The automatic equalizer, IR-MPPM demodulator, and data storage are implemented in the FPGA board. The total size is 26 cm × 10 cm.

than the ZF method. In contrast, the ZF method forces the receiver output to be zero at all the sampling instances, except for the time instant which corresponds to the transmitted signal. This is easier to be implemented by hardware, and we therefore adopted the ZF method in our receiver.

The ZF method is accomplished by a digital finite-impulse response (FIR) filter [11]. When input to the FIR filter is the discrete impulse response h_k of an implant communication channel, the output y_k can be expressed as a discrete convolution of the input h_k and the filter coefficient c_n

$$y_k = \sum_{n=-N}^{n=N} c_n \cdot h_{k-n} \tag{2}$$

where k is the sample number of the discretely sampled time signal and n is the filter tap number. The ZF method requires $y_k = 0$ for $k \neq 0$ and $y_k = 1$ for $k = 0$. Substituting this condition into (2) yields a set of $2N+1$ simultaneous equations

$$\begin{bmatrix} 0 \\ \vdots \\ 1 \\ \vdots \\ 0 \end{bmatrix} = \begin{bmatrix} h_0 & h_{-1} & \cdots & h_{-2N} \\ \vdots & \vdots & & \vdots \\ h_N & h_{N-1} & \cdots & h_{-N} \\ \vdots & \vdots & & \vdots \\ h_{2N} & h_{2N-1} & \cdots & h_0 \end{bmatrix} \begin{bmatrix} c_{-N} \\ \vdots \\ c_0 \\ \vdots \\ c_N \end{bmatrix}. \tag{3}$$

To derive the impulse response h_k, the transmitter periodically transmits a known signal sequence as the training signal for the equalizer. The training signal is a random "1" and "0" sequence of 4096 bits arranged between the start bits and the stop bits. By detecting the known sequence in the receiver and storing it in a memory, the transmitted and received training signals are recorded. Then, the equalizer calculates the frequency spectrum $R_x(f)$ of the transmitted training signal and $T_x(f)$ of the received training signal by using the fast Fourier transform (FFT), and derive the transfer function $H(f)$ from $R_x(f)/T_x(f)$. In such a way, we can derive the impulse response h_k by applying the inverse FFT to the transfer function $H(f)$, and obtain the filter coefficient c_n by solving

TABLE I
IR TRANSCEIVER SPECIFICATIONS

Pulse width	100 ns
Pulse number per bit	8, 4, 2, 1
Frequency band	10 - 60 MHz
Modulation	IR-MPPM
Data rate	1.25, 2.5, 5, 10 Mbps
Maximum output	~ 0 dBm
Demodulation	Envelope detection
Equalization method	ZF method

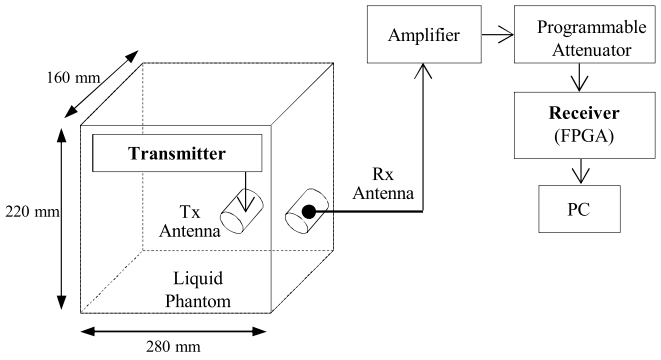

Fig. 8. Experimental setup in a biological-equivalent liquid phantom.

the set of (3) with the derived channel impulse response. Thus, the influence of the communication path can be canceled by the FIR filter from the received signal. Since the coefficients of the digital FIR filter are periodically updated, the receiver adapts to the channel characteristics in real time. After the automatic equalizer, the envelope of the equalized signal is extracted and is judged as chip "0" or "1" by a comparator. Then, they are further decoded to reproduce the transmitted information bits.

Table I summarizes the specifications of the developed transmitter and receiver. Both the transmitter and the receiver were implemented in an FPGA board. The FPGA's design language is Verilog-HDL which consists of a simulator to examine whether the designed transmitter and receiver codes work. After the debug in the simulator for an assumed received signal, the designed codes were written into the FPGA boards, and the FPGA boards worked as the transmitter and receiver, respectively. It should be noted that, since the maximum transmit power is around 0 dBm (1 mW), the localized 10-g averaged specific absorption rate will be much smaller than the general safety limit of 2 W/kg [12] even if we consider a worst case where the transmit power is completely absorbed in 10 g of human tissue. Fig. 8 shows the setup of experimental validation in a biological-equivalent liquid phantom as described in Section III. The transmitter together with either the helical dipole antenna or the helical invert-F antenna was wrapped with vinyl and inserted in the liquid phantom. The receiver together with the same type antenna was set on the phantom surface with a spacing of 5 mm, and connected to a personal computer via a USB interface for recording the received data and counting the BER. First, instead of a direct comparison of BERs between the FPGA simulator and the phantom experiment, we made a comparison between the simulated and measured ratios of the power received in the

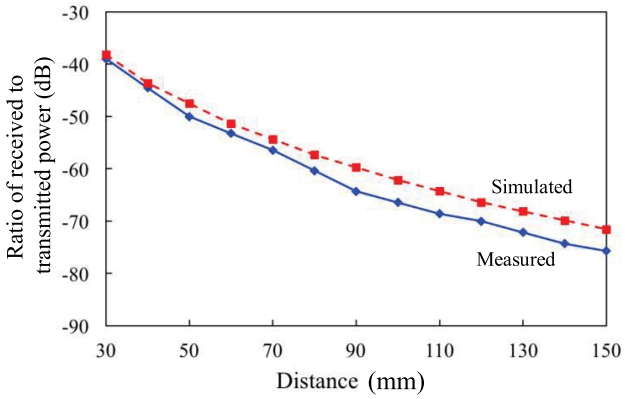

Fig. 9. Comparison between simulated and measured ratios of the power received in the FPGA-implemented receiver to the power transmitted from the FPGA-implemented transmitter for the helical invert-F antenna.

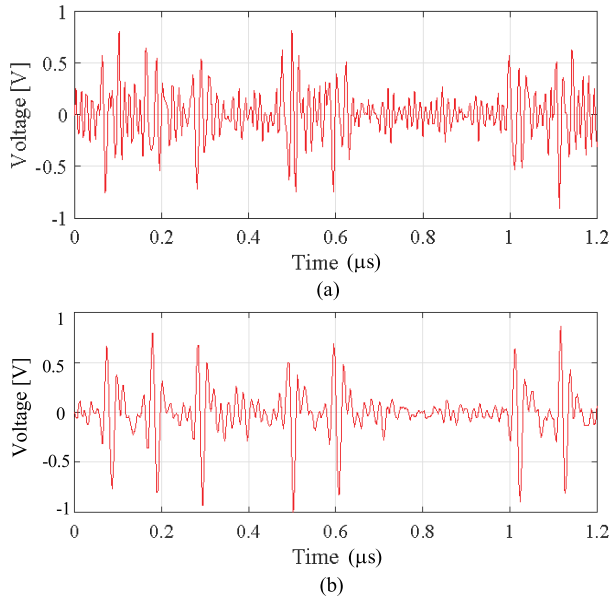

Fig. 10. Comparison of time waveforms of received signals. (a) Without equalization. (b) With equalization.

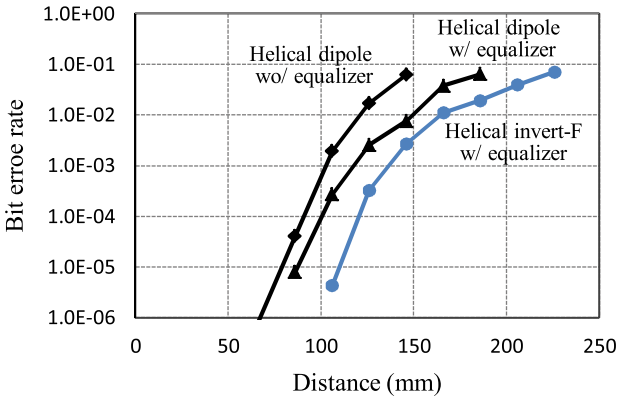

Fig. 11. Comparison of measured BERs for implant communication in the liquid phantom.

FPGA-implemented receiver to the power transmitted from the FPGA-implemented transmitter. Fig. 9 shows the results for the helical invert-F antenna. Although there are some

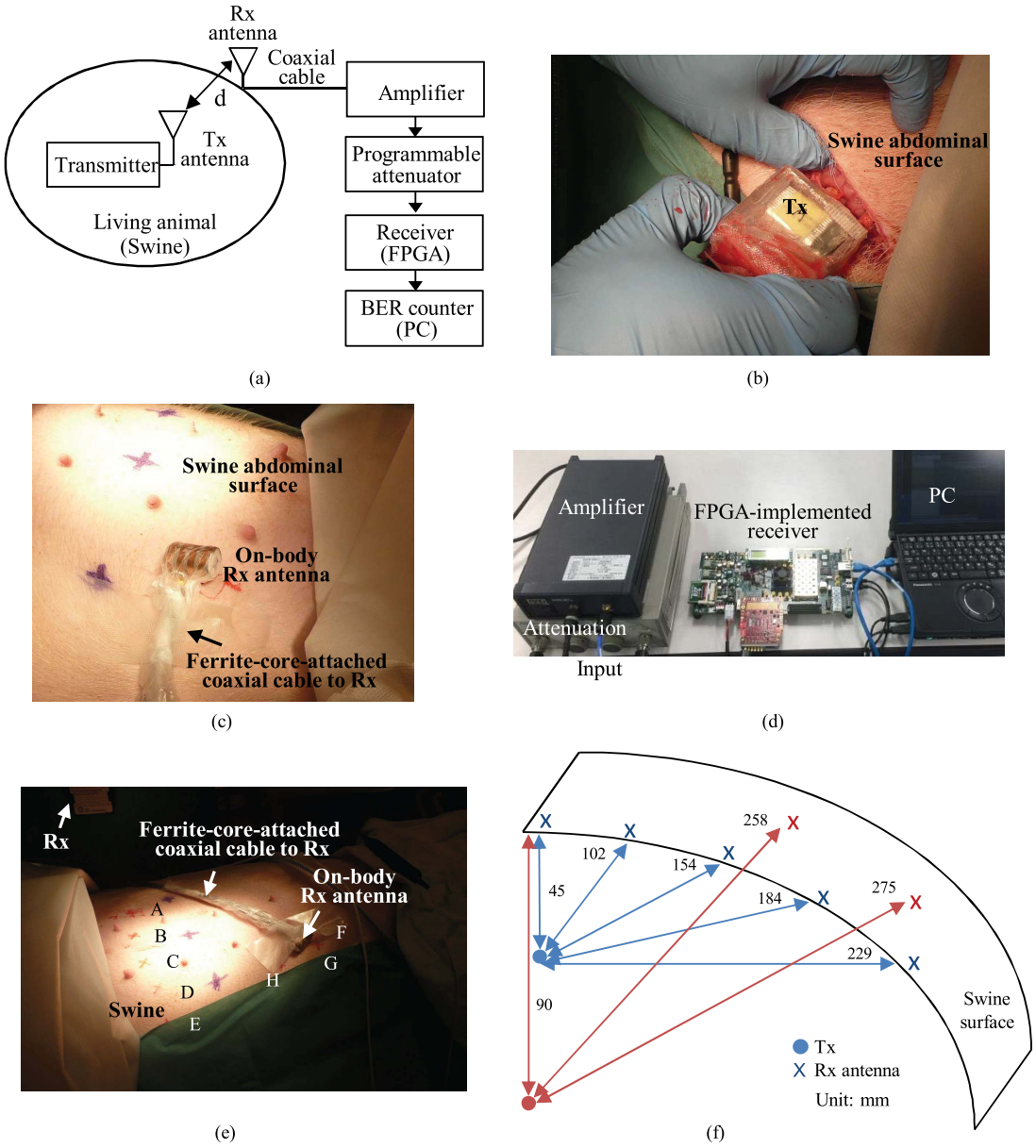

Fig. 12. *In vivo* experiment of implant communication. (a) Block diagram of the *in vivo* experiment with a living swine. (b) View of the implant transmitter to be inserted into the swine's abdomen. (c) View of a helical invert-F antenna for the receiver on the swine's abdominal surface. (d) Receiver consisting of an amplifier, a programmable attenuator, and an FPGA board. (e) View of the *in vivo* experiment consisting of the arrangement of the swine, the on-body receive antenna, and the receiver. The marks from A to G on the swine's abdominal surface: receive antenna positions. (f) Positions of the implant transmitter and the corresponding communication distances to the on-body receive antenna.

deviations between the FPGA simulator and experimental results as the communication distance increases, they are generally in agreement.

Then, to confirm the equalization effect, we measured the signal waveform before and after the equalizer at the receiver. Fig. 10 compares the input signals to the IR-MPPM demodulator with and without the equalizer. It is evident that, by comparing them with Fig. 4(a), the designed equalizer improves the signal quality and mitigates the intersymbol interference. The correlation coefficient with respect to the transmit signal was improved from 0.4 to 0.7 at a communication distance of 10 cm.

Fig. 11 shows the measured BER performance as a function of distance from the implant transmitter to the receive antenna on the phantom surface at a data rate of 10 Mb/s. As can be seen, the BER performance with the automatic equalizer was totally improved by nearly one digit and the communication distance is significantly extended compared to before. The best BER performance was obtained when the helical invert-F antenna was used. As a result, with the automatic equalizer, we accomplished a BER smaller than 10^{-2}, an acceptable BER level in the physical layer, at a communication distance of up to 16 cm for the data rate as high as 10 Mb/s.

V. *In Vivo* Experiment on a Living Swine

After the validation experiment of the biological-equivalent liquid phantom, we carried out an *in vivo* implant communication experiment on a living swine. The approval of the

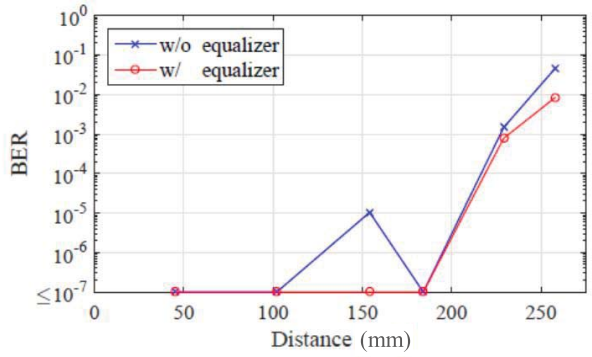

Fig. 13. Measured BERs versus communication distance at 10 Mb/s.

Norwegian Animal Research Authority was acquired before we carried out the living animal experiment at the Oslo University Hospital, Oslo, Norway. During the experiment, we provided humane treatment to the animal in accordance with the standard clinical protocol defined in Article 23 of EU Directive 2010/63.

Fig. 12 shows the *in vivo* experiment setup of implant communication. Fig. 12(a) is the block diagram of the *in vivo* experiment. Fig. 12(b) and (c) shows the implant transmitter to be inserted into the swine's abdomen and a helical invert-F antenna for the receiver on the swine's abdominal surface, respectively. Fig. 12(d) shows the receiver consisting of a low-noise amplifier, a programmable attenuator, and an FPGA board. Fig. 12(e) is an overview of the *in vivo* experiment consisting of the arrangement of the swine, the on-body receive antenna, and the receiver. The marks from A to G on the swine's abdominal surface denote the receive antenna positions. The abdomen of the swine was first laparotomized, and the developed implant transmitter together with the helical invert-F antenna, covered with vinyl for insulation, was inserted inside it at a depth of 4.5 and 9 cm, respectively. Then, the cut wound of the abdomen of swine was stitched for realizing an implant communication situation. The same type receive antenna on the swine's abdomen surface was connected to the receiver by a ferrite core-attached coaxial cable, and the receiver was connected to a personal computer via a USB interface for BER count. The communication distances between the implant transmitter and the on-body receive antenna were measured using an electromagnetic tracking system (NDI, Aurora). Once the implant transmitter position and the on-body receive antenna position were fixed, we first measured the distance between them using the electromagnetic tracking system, and then started the implant communication and BER measurement. The communication distances thus obtained are shown in Fig. 12(f). The main tissue types between the transmitter and the receiver antennas were small intestine, fat, muscle, and skin.

Fig. 13 shows the measured BER performances versus communication distance in the swine with and without the equalizer. The BER performance was improved by the equalizer at all communication distances. A BER smaller than 10^{-2} was accomplished up to 26 cm at 10 Mb/s. This result is somewhat better than that in the liquid phantom, and should be attributed to that the liquid phantom simulated tissue properties

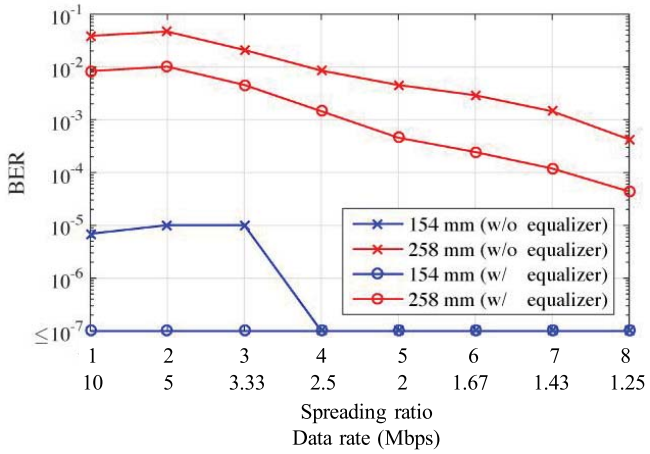

Fig. 14. Measured BERs for different data rates at various communication distances.

closer to muscle, yielding a path loss larger than what was seen in the swine's abdomen. Also, a BER degradation at 15 cm was observed in Fig. 13. This is because different communication routes consist of different tissue types and thicknesses. High water content tissue such as small intestine has larger path loss, whereas low water content tissue such as fat has smaller path loss. The implant communication performance is therefore dependent not only on the communication distance but also on the tissue types and thickness between the transmitter and the receiver. By using the automatic equalizer, this BER degradation was improved obviously.

Moreover, we evaluated the BER performance when multiple pulses were used to represent one bit for further improving the communication performance instead of sacrificing the data rate. The BER performances were obtained for various spreading ratios, in other words, different data rates. In this case, each information bit was encoded by a pn sequence with a spreading ratio from 1 to 8, which corresponded to data rates from 10 to 1.25 Mb/s. Fig. 14 shows the BER performance as a function of the spreading ratio from 1 to 8. As can be seen, the BER was obviously improved with the increase in spreading ratio or the decrease in data rate. For example, at the communication distance of 25.8 cm, the BER was improved from 10^{-2} to 10^{-3} by changing the spreading ratio from 1 to 4 (the data rate from 10 to 2.5 Mb/s) in the case with an equalizer. From Fig. 14, the BER can be secured below 10^{-2} up to a communication distance of 26 cm at a data rate of 2.5 Mb/s in the case without an equalizer and 10 Mb/s in the case with an equalizer. These *in vivo* experimental results demonstrated the highest data rate, which has been reported so far, in a communication distance as deep as 26 cm in a living body.

VI. Conclusion

There is a strong desire to develop high-speed, high-reliable wireless implant communication technology for various medical and healthcare applications. For this purpose, we have studied and developed an implant transceiver working at 10–60-MHz band with the employment of the IR technology using an MPPM scheme. By using an automatic equalizer

with the ZF method to suppress the waveform distortion and intersymbol interference due to frequency-dependent tissue properties, the correlation coefficient between the received signal and the transmitted signal has been improved from 0.4 to 0.7. By forming the antenna radiation elements on a flexible magnetic sheet to shorten the equivalent wavelength for antenna miniaturization, the implant antenna has been produced with a dimension of 2.6 cm × 1.6 cm × 1.6 cm and a relative bandwidth of 16%. Through the *in vivo* experiment on a living swine, we have achieved an implant communication performance with a BER smaller than 10^{-2} and a data rate as high as 10 Mb/s at a depth of up to 26 cm. The proposed implant transceiver has the best results reported so far in the literature in terms of transmitter power, data rate, and depth.

The future objective is to integrate the implant transceiver circuits into one module for practical use and verification.

REFERENCES

[1] *IEEE Standard for Local and Metropolitan Area Networks—Part 15.6: Wireless Body Area Networks*, IEEE Standard 802.15.6-2012, Feb. 2012.

[2] J. Wang and Q. Wang, *Body Area Communications: Channel Modeling, Communication Systems, and EMC*. Hoboken, NJ, USA: Wiley, 2012.

[3] E. Monton *et al.*, "Body area network for wireless patient monitoring," *IET Commun.*, vol. 2, no. 2, pp. 215–222, Feb. 2008.

[4] M. R. Yuce and T. Dissanayake, "Easy-to-swallow wireless telemetry," *IEEE Microw. Mag.*, vol. 13, no. 6, pp. 90–101, Sep. 2012.

[5] D. Anzai *et al.*, "Experimental evaluation of implant UWB-IR transmission with living animal for body area networks," *IEEE Trans. Microw. Theory Techn.*, vol. 62, no. 1, pp. 183–192, Jan. 2014.

[6] Y. Shimizu, D. Anzai, R. Chavez-Santiago, P. A. Floor, I. Balasingham, and J. Wang, "Performance evaluation of an ultra-wideband transmit diversity in a living animal experiment," *IEEE Trans. Microw. Theory Techn.*, vol. 65, no. 7, pp. 2596–2606, Jul. 2017.

[7] S. Gabriel, R. W. Lau, and C. Gabriel, "The dielectric properties of biological tissues: III. Parametric models for the dielectric spectrum of tissues," *Phys. Med. Biol.*, vol. 41, no. 11, pp. 2271–2293, 1996.

[8] C. Gabriel, "Compilation of the dielectric properties of body tissues at RF and microwave frequencies," Brooks Air Force, San Antonio, TX, USA, Tech. Rep. AL/OE-TR-1996-0037, 1996.

[9] (2015). *The Radio Use Website*, (in Japanese). [Online]. Available: http://www.tele.soumu.go.jp/j/ref/material/rule/

[10] J. Wang, J. Liu, K. Suguri, and D. Anzai, "An in-body impulse radio transceiver with implant antenna miniaturization at 30 MHz," *IEEE Microw. Wireless Compon. Lett.*, vol. 25, no. 7, pp. 484–486, Jul. 2015.

[11] S. S. Haykin, *Adaptive Filter Theory*, 2nd ed. Englewood Cliffs, NJ, USA: Prentice-Hall, 1996, pp. 217–220.

[12] *IEEE Standard for Safety Levels with Respect to Human Exposure to Radio Frequency Electromagnetic Fields, 3 kHz to 300 GHz*, IEEE Standard C95.1-2005, Oct. 2005.

Jianqing Wang (M'99) received the B.E. degree in electronic engineering from the Beijing Institute of Technology, Beijing, China, in 1984, and the M.E. and D.E. degrees in electrical and communication engineering from Tohoku University, Sendai, Japan, in 1988 and 1991, respectively.

He was a Research Associate with Tohoku University. He was a Senior Engineer with the Sophia Systems Company, Ltd. In 1997, he joined the Nagoya Institute of Technology, Nagoya, Japan, where he has been a Professor since 2005. He authored *Body Area Communications* (Wiley–IEEE, 2012). His current research interests include biomedical communications and electromagnetic compatibility.

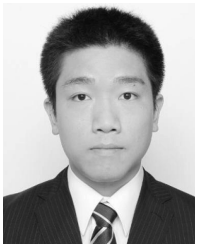

Kohei Nomura received the B.E. and M.E. degrees in electrical and electronic engineering with a focus on the study of implant communications from the Nagoya Institute of Technology, Nagoya, Japan, in 2016 and 2018, respectively.

He is currently with the Mitsubishi Electric Corporation, Kobe, Japan.

Hiroki Narita received the B.E. and M.E. degrees in electrical and electronic engineering with a focus on the study of implant communications from the Nagoya Institute of Technology, Nagoya, Japan, in 2014 and 2016, respectively.

He is currently with Aisin Seiki Co. Ltd., Aichi, Japan.

Fuminori Ito received the B.E. and M.E. degrees in electrical and electronic engineering with a focus on the study of implant antennas from the Nagoya Institute of Technology, Nagoya, Japan, in 2015 and 2017, respectively.

He is currently with the DENSO TECHNO Co. Ltd., Aichi, Japan.

Daisuke Anzai (S'06–A'11–M'14) received the B.E., M.E., and Ph.D. degrees from Osaka City University, Osaka, Japan, in 2006, 2008, and 2011, respectively.

Since 2011, he has been with the Graduate School of Engineering, Nagoya Institute of Technology, Nagoya, Japan, as an Assistant Professor, where he is currently an Associate Professor. His current research interests include biomedical communication systems and localization systems in wireless communication networks.

Dr. Anzai was a recipient of the 2015 IEEE MTT-S Japan Young Engineer Award and the Telecommunications Technology Award from the Telecommunications Advancement Foundation.

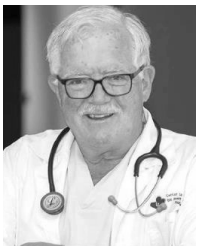

Jacob Bergsland received the medical and Ph.D. degrees, from Oslo University, Oslo, Norway, in 1973 and 2011, respectively.

Following an internship in Norway, he moved to the USA for education in surgery. In 1981, he became a Specialist in General Surgery and Cardiothoracic Surgery in 1983. He was the Director of Cardiac Surgery with the Buffalo VA Hospital, the Director of the Cardiac Transplantation Program with Buffalo General Hospital, the Director of the Center for Less Invasive Cardiac Surgery, and a Clinical Associate Professor of Surgery with the State University of New York, Buffalo, NY, USA. He was also the initiator of the hospital partnership between Buffalo General Hospital and the Tuzla Medical Center, Tuzla, Bosnia and Herzegovina, in 1995, and a developer of cardiovascular surgery and cardiology in Bosnia and Herzegovina. He is currently a Researcher and co-investigator with The Intervention Centre, Oslo University Hospital, Oslo, the Medical Director with the BH Heart Centre, Tuzla BIH, Tuzla, and the Medical Director with the Medical Device Company, Cardiomech AS. He has been a Project Leader for numerous humanitarian and scientific grants. He has authored or co-authored 148 peer-reviewed papers.

Ilangko Balasingham (S'91–M'98–SM'11) received the M.Sc. and Ph.D. degrees in signal processing from the Department of Electronics and Telecommunications, Norwegian University of Science and Technology (NTNU), Trondheim, Norway, in 1993 and 1998, respectively, and the master's degree from the Department of Electrical and Computer Engineering, University of California at Santa Barbara, Santa Barbara, CA, USA.

From 1998 to 2002, he was a Research Engineer with Fast Search & Transfer ASA, Oslo, Norway, which is now a part of Microsoft Inc., where he was involved in developing image and video streaming solutions for mobile handheld devices. Since 2002, he has been with The Intervention Center, Oslo University Hospital, Oslo, where he is currently the Head of the Section for Medical ICT Research and Development. He has also been a Professor of medical signal processing and communications with NTNU since 2006. From 2016 to 2017, he was a Professor with the Frontier Research Institute, Nagoya Institute of Technology, Nagoya, Japan. He has authored or co-authored over 225 journal and conference papers, 7 book chapters, 42 abstracts, and 20 papers in popular press. He holds six patents. His current research interests include super robust short-range communications for both in-body and on-body sensors, body area sensor networks, microwave short-range sensing of vital signs, short-range localization and tracking mobile sensors, and nanoscale communication networks.

Dr. Balasingham is a Steering Committee member of ACM NANOCOM from 2018 to 2021, and the General Chair of the 2019 IEEE International Symposium of Medical ICT. He was a Steering Committee member of the 2012 Body Area Networks Conference and a TPC Chair of the 2015 ACM NANOCOM. He has also given 16 invited/keynote presentations at international conferences. He has been an Area Editor of *Nano Communication Networks* (Elsevier) since 2013.